

## CFD Analysis of the Flow Between Dual-Layer Orthogonal-Offset Plate Arrays

R. A. Edgar<sup>1</sup>, S. Cochard<sup>2</sup>, Z. H. Stachurski<sup>1</sup>

<sup>1</sup>College of Engineering & Computer Science  
 Australian National University, Canberra 0200, Australia

<sup>2</sup>Faculty of Engineering & IT  
 The University of Sydney, Sydney 2006, Australia

### Abstract

Dual-layer orthogonal-offset plate (DLOOP) arrays are newly investigated arrangements of flat plates shown by numerical simulation to have lower drag, over a range of layer distances, than contiguous plates of equivalent frontal area at high angles of attack.

The DLOOP arrangement takes the contiguous area of a virtual plate, divides it into smaller sub-sections and relocates each alternate sub-section to the alternate layer so that none remain side-by-side. For example, a square *chessboard* DLOOP assembly has an upper-layer of thirty-two *black* plates overlapping a layer of thirty-two *white* plates. The chessboard's orthogonal offset, between plates of overlapping layers, results in zero overlap between individual plates which is a significant feature for solar tracking power systems to combine more photovoltaic panels in a way that can resist higher wind specifications.

### Introduction

The subset of dual-layer orthogonal-offset plate (DLOOP) arrays investigated in this paper have square layer envelopes and plates; and the plates of each layer meet at corners and not along sides. This subset includes the *chessboard* DLOOP array, henceforth called the  $8 \times 8$  array, and other similar forms having plates in *black*-overlying-*white* square positions which are variously called  $9 \times 9$ , ...  $4 \times 4$  arrays, depending on their horizontal and vertical plate counts.

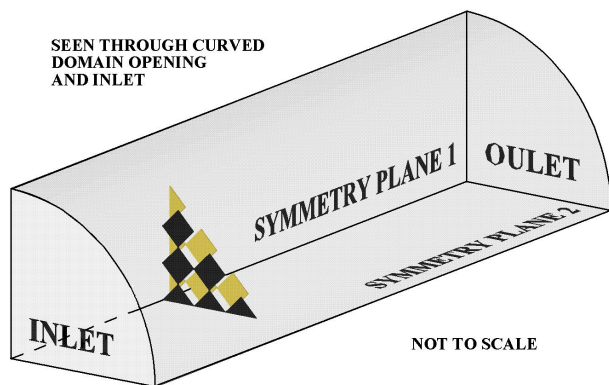


Figure 1: General layout of analysis domain

Of interest in this paper are the maximum forces exerted by fluids on these arrays. The ANSYS 14.0 CFX commercial software package with the  $k-\omega$  Shear Stress Transport (SST) turbulence model [3], is used to report the drag of plate arrays placed perpendicular to what would be, in the absence of those arrays, *quasi-steady* incompressible isotropic turbulent flows. Depending on whether the characteristic length is taken to be the plate or array envelope side lengths, the Reynolds numbers of the flows investigated are in the order of  $10^6$  to  $10^7$ .

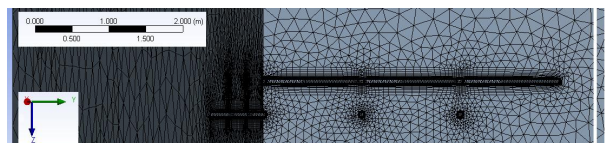


Figure 2: Mesh detail on left/right symmetry planes

### Methods

The report has a baseline array envelope of  $5.74 \text{ m} \times 5.74 \text{ m}$  and uses 46 mm thick plates. The impinging flow is air ( $\rho = 1.185 \text{ kg.m}^{-3}$ ;  $\mu = 1.831 \times 10^{-5} \text{ kg m}^{-1} \text{ s}^{-1}$ ) with an average velocity of  $35 \text{ m s}^{-1}$  travelling perpendicular, i.e. face-on, to the plates and with turbulent velocity components of magnitude 10% rms.

In order to significantly reduce the computational overhead of the analysis, the diagonal (or for odd arrays possible mid-side) geometric symmetry of arrays was extended to the computational domain by assuming two orthogonal axes of mirror symmetry. This enabled results to be obtained quickly by modelling just one quarter of the domain otherwise required. While recognising that real world conditions with geometric symmetry won't necessarily have symmetric flow patterns, the computational advantage of the approach was adopted on the basis that:

- the flow windward of the DLOOP assembly would be largely symmetric with only the sheltered, slower and less forceful average leeward flows exhibiting transient asymmetries;
- the SST is an isometric Reynolds averaged Navier-Stokes equation approach that will average out flow asymmetries in the baseline steady state analyses anyway; and
- results can be audited by running a transient analysis of the full geometry, i.e. without symmetry, for some arrangements as required.

The general layout of the  $6 \times 6$  array's domain is shown NOT TO SCALE in Figure 1. The domain in particular is proportionally much larger than presented in the figure for clarity. The analysis domain is a quarter cylinder with its axis orientated in the direction of the *inlet*'s quasi-steady flow and passing through the symmetric centre of the DLOOP array. The quarter disk area of the analysis domain's *inlet* and *outlet* are each  $36 \times$  that presented by the quarter array's frontal surface. The analysis domain's axis is  $15 \times$  the array envelope's side length plus the inter-layer distance of the enclosed array. The planes of the array's symmetric centre are 5 array-side-lengths from the inlet and 10 array-side-lengths from the outlet.

A tetrahedral mesh of 0.5 m maximum face size on domain surfaces and maximum 0.6 m otherwise fills the bulk of the analy-

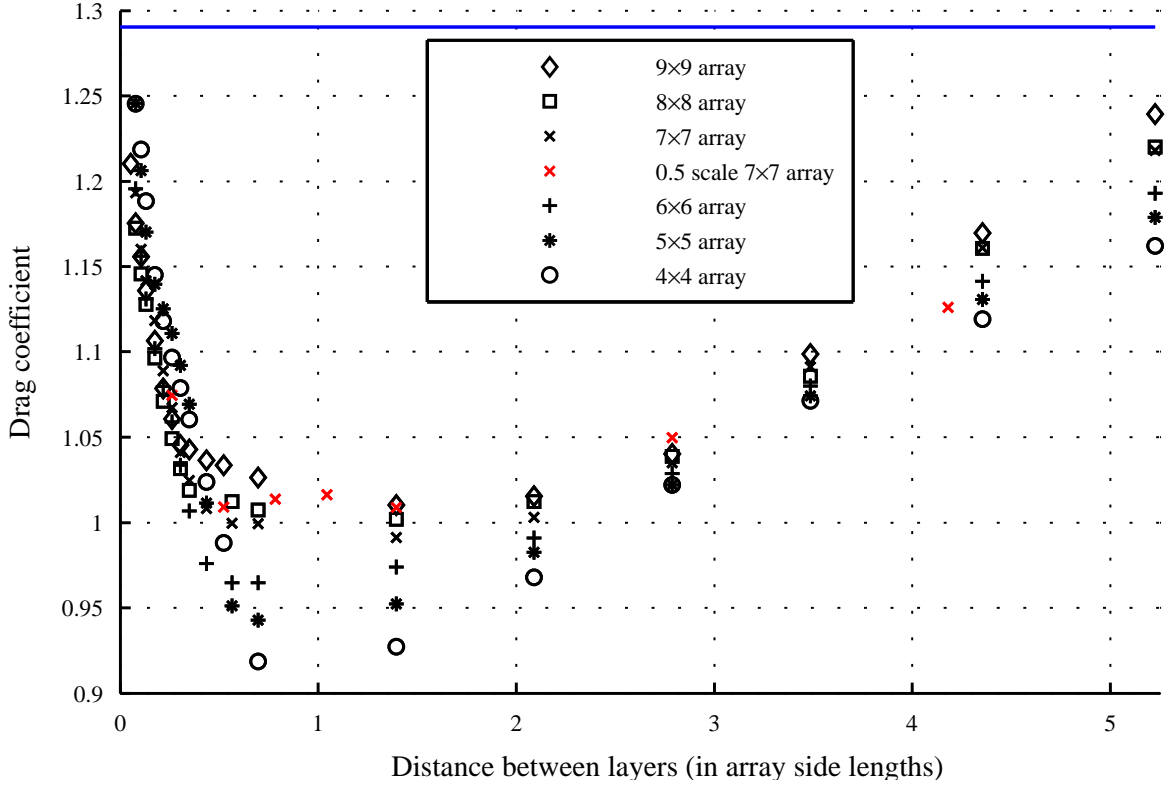


Figure 3: Drag on DLOOP arrays

sis domain. The remaining volume has smaller mesh sizes and surrounds arrays. The latter includes prisms in 15 surface inflation layers and proximity mesh sizing of 46 mm at array edges expanding with 1.2 growth rate. The 1<sup>st</sup> inflation layer is 2 mm thick in order to keep  $Y^+ < 30$  and have the wall functions modelling the subtle effects of the viscous sub-layer effectively. A detail figure showing the mesh on the symmetric plane surfaces of the  $6 \times 6$  array domain is given in Figure 2.

When audits of particular baseline results were undertaken with the full geometry modelled, i.e. a transient analysis without use of any domain symmetry, the relevant time-step was chosen in the order of  $10^{-4}$  s to keep the average courant number below one and have the flow evolving at a rate compatible with mesh sizes. The chosen time-step also allowed the solution momentum residuals to approach or better  $1.5 \times 10^{-5}$  rms-relative within the specified allowance of 15 iterations per time-step.

## Results

The drag results of the baseline DLOOP array analysis are shown in Figure 3. The red markers in Figure 3 indicate results obtained with a half cross-wind scale  $7 \times 7$  array, i.e. one having a  $2.87 \text{ m} \times 2.87 \text{ m}$  envelope but 46 mm plate thickness maintained. The interlayer distances, i.e. orthogonal distance between the arrays' layers, were varied over about 5.25 array envelope-side-lengths (equivalent to 30 m for the baseline) to identify drag minima distances and trends. A blue line on the same figure indicates the analysis' reported higher drag of a contiguous flat plate having equivalent frontal area to that of the baseline arrays.

Figure 4 shows physically measured drag results for square plates reported over an extensive Reynolds number range by

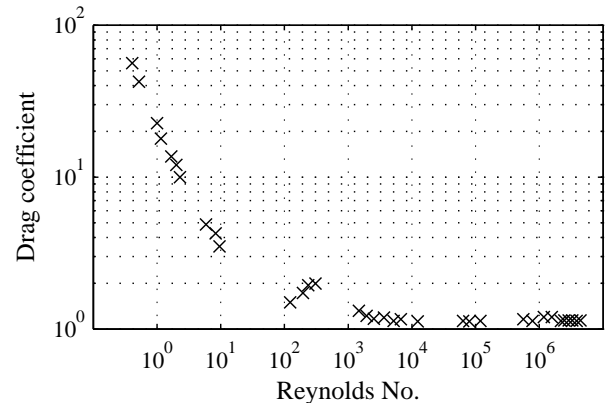


Figure 4: Drag measured on square plates, reported by Hoerner [2]

Hoerner[2, Fig.3-26]. Plate drag increases have been observed and measured as high as 4% with turbulence [4], but the SST result shown by the blue line in Figure 3 is still  $\approx 6\%$  above that given, as shown in Figure 4,  $C_D = 1.17$  has been measured for non-turbulent conditions in this Reynolds number range.

As a result of the higher than expected square plate drag  $C_D = 1.29$  reported in the baseline analysis, four additional audit analyses relating to the contiguous square plate were undertaken:

1. a quarter square plate was formed for analysis from mid-side symmetry planes rather than the diagonal ones of the baseline which is shown with a  $6 \times 6$  array in Figure 1, i.e. results in a square frontal profile instead of triangular one

while surface area is kept constant – obtained essentially identical results to those of the baseline reported in item (4) below;

2. the baseline analysis domain was re-meshed with half maximum geometric size settings, half the proximity growth rate and twice as many inflation layers – obtained essentially identical results to those of the baseline reported in item (4) below;
3. a full square plate transient analysis without symmetry was undertaken having a cylindrical analysis domain, i.e. comprised all four quarters, each basically equivalent to the baseline domain – expended several orders of magnitude more computational resources and reported  $C_D = 1.276 \pm 0.006$  or about 1.0% lower drag than the baseline; and
4. a detailed review of the baseline steady state results (and those of audit items (1) and (2) above) over its latter 100 pseudo timesteps (0.25 s each) when the average drag force and oscillations had stabilised – showed  $C_D = 1.22 \pm 0.09$ .

Noting the marginal difference of audit outcomes, the original blue line for contiguous plate drag  $C_D = 1.29$  was preserved in Figure 3 in order to keep and compare analysis results based on like computational methods. Despite this, work is ongoing by the authors to compare matches between analysis and experiment for globally unstable flows head on to plates at high Reynolds number ranges using scale-resolving simulations.

A consistent minima in the drag coefficient of the DLOOP arrays is revealed in Figure 3 for inter-layer distance in the region of one array envelope-side-length apart. In general, the less dense array plate grids analysed showed the lowest drag coefficient for inter-layer distances greater than approximately three-quarters of an array envelope-side-length apart. By contrast, the drag trends of Figure 3 become mixed and are generally reversed for smaller layer distances, with the more dense array plate grids showing the lowest drag coefficient at distances below the order of their constituent plate-side-lengths apart.

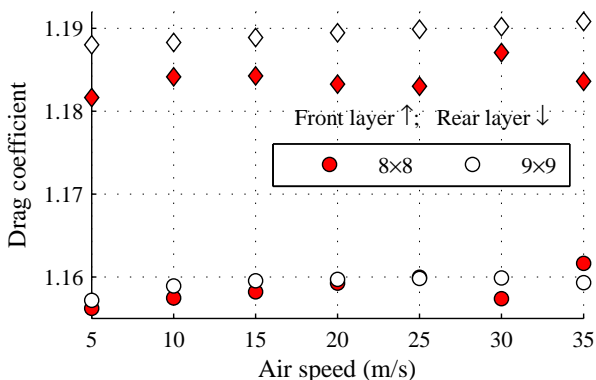


Figure 5: Drag of arrays with 450 mm between layers

In Figure 3 there is a reasonable consistency shown between the half scale  $7 \times 7$  array's results, shown in red, and the baseline trend. The physics of the fluid therefore scale according to the Reynolds number of the conditions well. This observation is additionally supported by the results shown in Figure 5, where the fluid velocity (and Reynolds number) range has been varied by 700% and the drag coefficients of the  $8 \times 8$  and  $9 \times 9$  arrays has changed by  $< 0.5\%$ .

The drag results shown in Figure 6 are of the same baseline analysis reported in Figure 3 however the drag coefficients of the arrays' front and rear layers are reported separately.

The results of Figure 6 are remarkable in terms of the consistent series of drag trends it displays and particularly outside the inter-layer distance of individual plate-side-length scales. For arrays with an inter-layer distance above their constituent plate-side-length apart, the drag coefficient of:

- windward layers rises asymptotically to a peak, and the more dense the arrays' plate grids the nearer these drags approach the level of a long flat rectangular plate, or stalled wing, at  $90^\circ$  angle-of-attack having  $C_D = 1.9$ ; and
- leeward layers is a minimum when the inter-layer distance is  $\approx 1.25$  envelope-side-lengths in scale.

To understand the above results it is convenient to think of the layers with the highest plate grid density providing the best shelter, so in an array that translates to higher relative drag on windward layers of arrays with the highest plate grid, and this gives better shelter to their leeward layers that then have lesser drag. For example the  $9 \times 9$  array will have higher drag on its windward layer and lower drag on its leeward layer relative to the  $8 \times 8$  etc..

More difficult to see in Figure 6 is the drag behaviour of the windward layer of arrays at low inter-layer distances, i.e. at or below their individual plate-side-length scale. There is an initial drop in the drag coefficient of the windward layer at short inter-layer distances before the more general rise of that layer's drag at higher inter-layer distances takes effect. This suggests for solar applications there may be a sweet spot for short inter-layer distances where the drag contribution of both the front and back layers is below the level of the area equivalent flat plate and their combined force on the assembly significantly lower accordingly. This has been explained in earlier research by the authors [1], and demonstrates the reduced pressure differential that can occur across windward layers at short layer distances when back pressure is able to build up on the windward face of a nearby leeward layer.

## Conclusions

This work is ongoing but the general drag trends for square dual layers of orthogonal offset plate arrays appears clear for those having an inter-layer distance greater than the scale of the individual plate-side-length concerned. The SST analysis shows DLOOP drag is significantly reduced relative to contiguous plates of equivalent area.

For closely packed DLOOP arrays, with inter-layer distances in the order of, or below, their constituent plate-side-length in scale, significant small scale turbulent flow structures are possible. These small scale structures may lead to highly energetic flows between densely packed DLOOP layers, allowing more exceptions to the general drag trends to emerge according to geometric coincidences concerned. Only more detailed transient analyses, including other than Reynolds averaged Navier-Stokes model approaches, of these closely packed arrays will improve the predictability of their flow structures and effects.

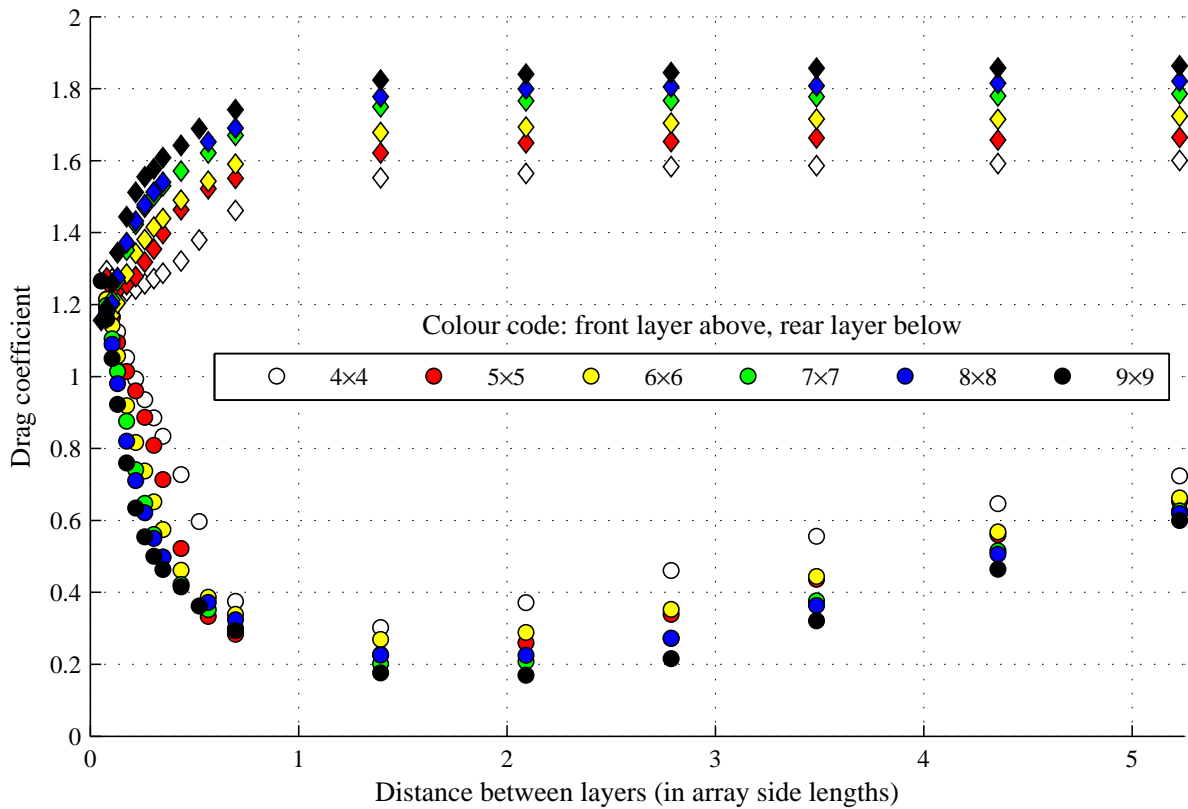


Figure 6: Drag distribution on front and rear layer of DLOOP arrays

## References

- [1] Edgar, R., Cochard, S. and Stachurski, Z., *Wind loads on solar panels in dual-layer offset-plate arrangements*, 15<sup>th</sup> Australian Wind Engineering Society: Workshop proceedings, 2012.
- [2] Hoerner, S. F., *Fluid-dynamic drag*, S.F.Hoerner, 1951, 2<sup>nd</sup> Ed. 1965.
- [3] Menter, F. R., Two-equation eddy-viscosity turbulence models for engineering applications, Technical Report 32(8): 1598-1605, American Institute of Aeronautics and Astronautics Inc., 1994.
- [4] Schubauer, G. B. and Dryden, H. L., The effect of turbulence on the drag of flat plates, *NACA Technical Report*, 129-133.